(Received 15 November 2023, Accepted 27 December 2023, Scheduled January 11, 2024)

A Review of the Advancement of Metasurfaces in Wearable Antenna Design for OFF-Body Communications

Nibash K. Sahu[1*], Naresh C. Naik[1], Madhab C. Tripathy[1], and Sanjeev K. Mishra[2]

[1] *Department of Electronics & Instrumentation Engineering, Odisha University of Technology and Research Bhubaneswar, Odisha, India*
[2] *Department of Electronics & Telecommunication, International Institute of Information and Technology Bhubaneswar, India*

ABSTRACT: This review article explores the advancement of metasurfaces in wearable antenna design for off-body communications. The wearable antenna needs to be compact, flexible, and, most importantly, should have less back radiation. In this context, wearable antennas that are inspired by metasurfaces are a good choice. Metasurface can make the antenna compact and reduce the back-radiated waves, which lowers the specific absorption rate (SAR) and improves the antenna's performance. In addition, the metasurface can also generate circular polarization (CP) by carefully rotating the electromagnetic (EM) waves incident on it and multi-band by simultaneously exciting its multiple modes. Using the aforementioned features provided by the metasurface, the surveys are segregated as single-band with linear polarizations (LP), single-band with CP, dual-band with LP, dual-band with dual polarization, and dual-band with dual CP. Prior to the survey, the challenges and considerations for wearable antenna design as well as the theoretical perspective behind performance improvements are discussed. Also, a conventional unit-cell of the metasurface is theoretically designed using the discussed theories and validated using CST Microwave Studio, which shows good agreement with each other.

1. INTRODUCTION

In the modern era of technology, the development of wireless communication has increased rapidly to have faster and more reliable services, which helps to radically alter the way the world functions and runs for the benefit of mankind. Subsequently, there is a need for the development of Wireless Body Area Networks (WBAN) that connect various electronic devices worn on the human body [1–3]. WBANs are established in many circumstances in our day-to-day lives, as shown in Figure 1, and those are in the medical field, military, entertainment field, personal peripheral devices, corporate sector, security and rescue field, sport industries, etc. [4–7]. The communications in WBAN are divided into three types: on-body (OB) communication, where information is sent between the devices situated in the same human body; in-body communication, where information is sent from the outside of the body to the inside; and off-body communication, where information is sent from the devices situated on the body to the exterior of the body. These wireless communications are established with the help of wearable antennas. The antenna that is developed specially to be worn on the human body is known as a wearable antenna [3–7]. The physical integration of wearable antennas on the human body presents designers with a number of challenges. In order to integrate and fit into the body, antennas with planar geometry are the best choice for wearable applications. Consequently, In the last few decades, researchers have focused on the development of planar structures such as printed monopole antennas, cavity-backed antennas, planar inverted-F antennas (PIFA), and slot antennas [7–9]. They have designed the antennas over flexible substrates such as textiles, polyimides, papers, and composite materials to enable flexibility and conformability during bending and crumpling. However, the primary problems with these antennas are their enormous lateral size and, most importantly, their strong back radiation directly focus towards the human body. The body's absorption of EM energy may cause uninvited, adversative biotic effects. Additionally, the human body's close proximity to the antenna affects its overall performance.

To overcome these, an antenna with a high front to back ratio (FBR) is desired, such as the microstrip antenna baked by metallic ground [10–12] or the quarter-wavelength monopole antenna backed by reflectors [13, 14]. In the case of microstrip patch antenna, the ground plane functions as a rear shield, isolating the antenna from the body. Therefore, the human organism absorbs very little energy. However, microstrip patch antennas possess a narrow impedance bandwidth (BW), which might not be able to cover the required bands due to the shifting of frequency bands during various bending conditions induced by body deformation or motion. These problems can be solved using a wide range of operating frequencies, and in this scenario, monopole antennas backed by reflectors are the best choice. The monopole antenna provides a wide impedance bandwidth, and the reflectors reduce the back-radiation by reflecting it in the uni-direction. Two types of reflectors are mainly used which are perfect-electric-conductor (PEC) and perfect-magnetic-conductor (PMC)-like reflector. While PEC is used, it should be placed at a distance greater than quarter wavelength from the printed monopole antenna (MA) [13] to

* Corresponding author: Nibash Kumar Sahu (nibash11@gmail.com).

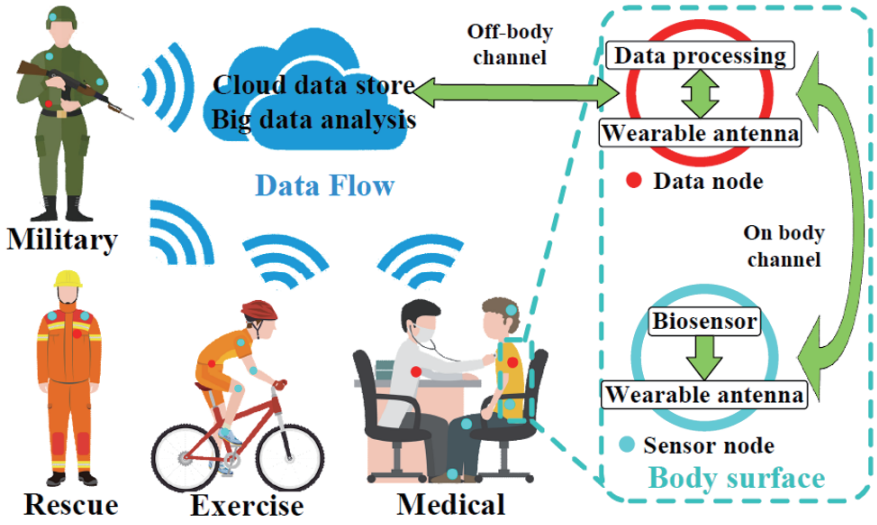

FIGURE 1. An overview of WBAN applications [6].

get in-phase reflection, which increases the overall foot prints. On the other hand, the PMC-like reflector can have the ability to provide in-phase reflection due to its in-phase parallel electric currents in close proximity to the actual currents. This possesses a high surface impedance, which makes the reflection phase of 0° at resonance. As PMC is not available in nature, PMC-like behavior is achieved by arranging the PECs in a periodic manner, which is called a metamaterial. The periodic arrangement can take three forms: three-dimensional (3-D), two-dimensional (2-D), or one-dimensional (1-D). Because of their ease of fabrication and flexibility, 2-D PEC arrangements are commonly used as reflectors. The 2-D arrangement over a surface is called a metasurface [14–19]. The use of a metasurface beneath a MA reduces the backward radiation, which in turn improves the impedance bandwidth, radiation efficiency, realized gain, and, most importantly, reduces the SAR to a safe value. In addition to being used as a reflector for back radiation reduction, the metasurface can also be used to generate dual-band and CP characteristics [18]. The fact is that the dual-mode operation of metasurface generates dual-frequency bands, and the polarization rotating features of metasurface generate circular polarizations. The CP characteristics overcome the polarization mismatch loss associated with linear polarization (LP) and make the signal more stable in realistic moving scenarios of the human body. Similarly, dual-band operation reduces the complexity and cost of integration compared to single-band operation and also increases the functionality of the devices. To demonstrate the advancements of metasurfaces for performance enhancement in wearable applications based on back radiation reduction, a review article [7] was presented. The article also covered the design methodology of metasurfaces and the material used in wearable antenna design. There is a high demand for review articles pertaining to performance enhancement using multifunctional metasurfaces in wearable applications.

In this review article, the advancements in metasurface-inspired antennas are discussed thoroughly. The review is segregated into single-band with LP, single-band with CP, dual-band with LP, dual-band with dual-polarization, and dual-band with dual CP. Prior to that, the design methodology of wearable antennas, followed by the difficulties that arise due to the placement of wearable antennas on the body and their overcome processes, are discussed. In addition, the theoretical perspective behind performance improvements is also discussed, along with a proposed theoretically developed unit cell of metasurface to resonate at 2.45 GHz. The structure of the paper is as follows. In Section 2, the design methodology for wearable antennas is discussed. In Section 3, the challenges that arise from the placement of these wearable antennas on the body are discussed, and in Section 4, the solutions are presented. Section 5 develops a unit cell of metasurface theoretically. Then Section 5 discusses the advancement in metasurface-inspired antennas for OFF-body communication, followed by a conclusion.

2. WEARABLE ANTENNA DESIGN

For designing a wearable antenna, the substrate and supporting layers must be made of a dielectric material, while the radiating elements such as patches, feeding lines, and ground plane must be made of conducting materials. These dielectric and conducting materials have been carefully chosen to provide an acceptable level of mechanical distortion while also being resistant to the effects of temperature, humidity, and radiation from electromagnetic fields. As a result, the wearable antenna will guarantee the user's comfort and security [7].

2.1. Dielectric Material Selection

In wearable applications, the antenna needs to be flexible to be comfortably worn on the body. Therefore, to achieve flexibility, it is necessary to fabricate the antenna using a flexible substrate rather than a rigid substrate. Careful selection of these flexible substrates can ensure that they continue to deliver a comfortable experience even when being bent, twisted,

TABLE 1. Dielectric material used in wearable applications with their electrical parameters.

Reference	Material.	ε_r	tan δ	Thickness (mm)
[6]	-	2.65	0.0027	3, 1.5
[8]	Rogers RT/duroid 5880	2.2	0.0009	0.127
[9]	Foam	1.495	0.016	3.7
[11]	Foam	1.52	0.012	3.94
[10]	Felt	1.38	0.02	1.1
[13–18]	Felt	1.6	0.044	1.5 &3.5
[20–22]	Felt	1.2	0.02	2.50& 3
[23]	Felt	1.3	0.044	3
[24]	Felt	1.2	0.044	3
[13]	Rogers RO4003C	3.38	0.0027	0.813
[20]	Jeans	1.6	0.04	2.5 & 3
[25]	Jeans	1.7	0.04	0.7
[20] & [26]	Cordura	1.9	0.0098	2.5 & 3
[27] & [28]	Paper	-	-	0.54 & 0.23
[29] & [30]	Denim	1.7	0.02	0.7
	Silk	1.75	0.012	-
[31]	PTFE	1.17 to 2.12	0.05	-
[26]	Quartzel Fabric	1.95	0.0004	-
[26]	Lycra	1.5	0.0093	-
[32]	Polymide	3.5	0.027	0.05
[33]	Kapton polyimide	3.5	0.002	
[33]	vinyl	2.5	-	1.5
[34]	Rogers RO3003	3	0.0013	1.50& 0.5
[35]	Pellon Fabric	1.08	0.008	3.6
[36]	Pellon Fabric	1.08	0.008	1.8
[37] & [38]	PDMS	2.7 & 2.9	0.013 & 0.02	2 & 3.5
[26]	Cotton	1.6	0.04	-
	Moleskin	1.45	0.05	
[20] & [26]	Polyester	1.9	0.0045	2.5 & 3
	Velcro	1.34	0.006	

stretched, crumpled, or otherwise deformed. Also, when choosing a substrate, the designer has to think about its thickness, permittivity, and tangent loss. The permittivity and thickness affect the impedance BW, whereas the loss-tangent affects the radiation-efficiency. An antenna with a low tangent loss and a high dielectric constant performs better [7]. However, the problems with fabric and textile substrate are that the dielectric constant tangent loss is frequency dependent. Thus, prior to the construction of a fabric antenna, a comprehensive evaluation of the characteristics of fabric substrates is necessary. Table 1 summarizes available flexible materials with their electrical properties.

2.2. Conducting Material Selection

For flexibility, the conducting portion of wearable antennas is frequently constructed from textile conducting materials. Consequently, it is essential to define their electrical properties. Additionally, it is essential to employ the proper material for the conductor to enhance the antenna radiation features and preserve the operation of the garment. In addition, care must be taken with manufacturing and packaging, as antenna design performance standards are directly influenced by the conductivity of the different materials used for manufacturing and packaging. The material conductivity (σ_m) can be derived with a known value of resistivity of the surface (ρ_{ms}) and substrate thickness (t_m) as follows:

$$\sigma_m = \frac{1}{\rho_{ms} t_m} \tag{1}$$

According to Equation (1), as resistance decreases, conductivity increases. Additionally, a decrease in resistivity reduces electrical losses and increases antenna efficiency. Several conductive materials are calculated and presented in Table 2 based

TABLE 2. Conducting material used in wearable applications with their electrical parameters.

Reference	Material.	ρ_{ms} (Ω/square)	σ_m (S/m)	t_m (mm)
[9]	Taffeta Fabric	0.18	-	0.08
[27] & [35]	Copper tape	–	$5.88 * 10^7$	0.03
[23] & [29]	Shieldit Fabric	-	$1.18 * 10^5$	0.17
[11]	Shieldit Fabric	< 0.1 0.18	$1.18 * 10^5$	0.17
[10]	FlecTron	< 0.1 0.18	-	0.17
[10]	Zelt	0.01	$1 * 10^6$	0.06
[21, 22]	Nora-Dell-CR Fabric	< 0.009	-	0.13
[36]	Taffeta Fabric	-	$2.5 * 10^5$	0.08
[38]	PDMS	-	$8.1 * 10^5$	0.1
[31]	Zelt	0.01	$1 * 10^6$	0.06

on Equation (1). Thus, for efficient EM radiation reception and transmission by the wearable antenna, the substrate dielectric material should have low loss, and the radiating element conductors should have high conductivity.

3. PLACING OF ANTENNA ON THE BODY AND ITS EFFECTS

The impact of EM radiation around human tissue is a crucial and difficult factor that researchers must take into account. The human body is a highly dispersive, lossy material with high dielectric constants that absorbs an enormous quantity of EM energy radiated by an antenna. The body's absorption of EM energy may result in unfavorable biological effects. The quantity SAR measures the quantity of energy absorbed by the human body. Typically, the SAR measurement requires averaging measurements over the entire body or a limited sample size. The SAR can be determined using the following equations [16] and [23]:

$$SAR = \frac{\sigma_b \left|E_b^2\right|}{\rho_b} \quad (\mathrm{W/Kg}) \tag{2}$$

$$SAR = \frac{d}{dt}\left(\frac{dW}{\rho dV}\right) \quad (\mathrm{W/Kg}) \tag{3}$$

where σ_b = body conductivity, ρ_b = body mass density, E_b = absorbed E-field by body, W = absorption of energy of human tissue, and V = sample volume.

Due to the global awareness of the health hazards, researchers and scientists are frequently interested in minimizing the body's absorption of energy or reaching the lowest SAR feasible. To safeguard the people, the US Federal Communications Commission (FCC) has set a limit of 1.6 W/Kg for 1 g standard SAR, while the EU commission has set a limit of 2 W/Kg for 10 g standard SAR [16–18]. Moreover, the dielectric constant, mass density, and conductivity are frequency-dependent, as a result of which the on-body antenna performances degraded [26]. Therefore, human-body and antenna interaction must be taken care.

The researchers and academics have created phantoms to account for the body effect, as shown in Figure 2. These phantoms are modelled numerically using any computational software, such as CST Studio and HFSS, or physically by employing a genuine physical structure [3]. The use of such nonhomogeneous and complex phantoms provides exact EM field measuring results. However, these phantoms necessitate a substantial number of processing resources for numerical simulations, including voxel models [32]. In contrast, it is easy to make a 3D-model of a portion of the human body instead of a whole phantom in the simulating software, which saves time and makes the design simpler. These 3D models are composed of stacked multilayer tissues with different shapes, sizes, and electrical characteristics for different parts of the body. For instance, the arm is accounted for by taking the stacks of cylindrical multilayer tissues such as 13 mm thick bone, 20 mm thick muscle, 5 mm thick fat, and 2 mm thick skin [27] as shown in Figure 2. A rectangular body model with the same tissue layers is employed in [25] to account for the chest. The authors of [24] have excluded the bottom layers that are bone to account for the chest. Figure 2 depicts the schematic of a brain model where a spherical stacking of tissue layers such as 80 mm thick brain, 2 mm thick CSF (Cerebro Spinal Fluid), 1 mm thick Dura, 10 mm thick skull, 4 mm thick muscle, 1 mm thick fat, and 2 mm thick skin have been used in [39].

4. OVERCOME OF BODY EFFECT

To overcome the unwanted body effects, the backward radiation needs to be minimized. For that, the antennas need to use reflectors like PEC and PMC. To understand the reflection mechanism clearly from a PEC and PMC surface [14], the image of the actual current due to the presence of these reflectors and their reflection mechanism are depicted is Figure 3. The fact is that the image of actual currents due to PEC reflectors is 180° out of phase, which indicates a reflection coefficient of -1. The reflected waves are therefore out of phase with the incident waves. As a result, destructive nature of interference arises, and performance as a whole decreases. To get in-phase reflection from PEC, it should be used at a distance greater than a quarter wave length from the printed MA [14]. On the other hand, a PMC reflector has in-phase image currents with the actual currents, which indicates a reflection coefficient of $+1$.

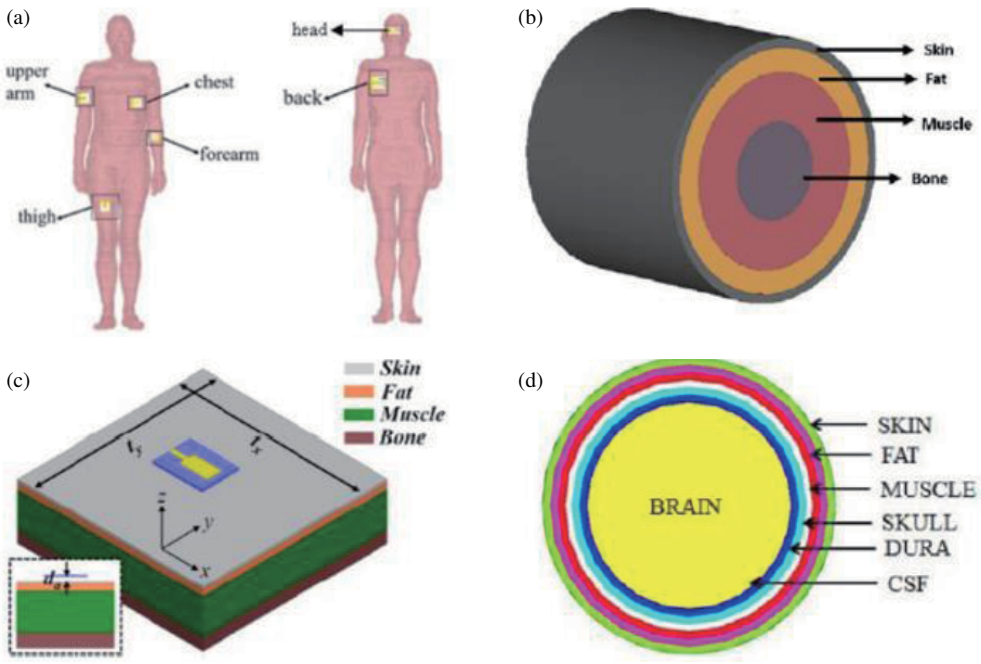

FIGURE 2. Schematic of (a) Human Voxel Model Phantom [32], (b) Arm Model [27], (c) Chest Model [25], and (d) Head Model [44].

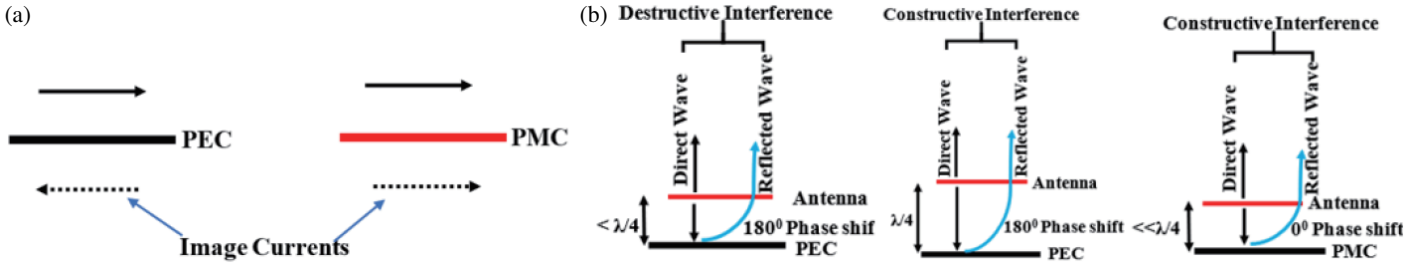

FIGURE 3. (a) Orientation of image current over PEC and PMC surface, (b) Reflection mechanism of PEC and PMC surface.

As a result, the accumulated radiated fields are in-phase, making impedance matching for the antenna seem less challenging even if it is in close proximity to the radiating antenna. Thus, constructive nature of interference arises, which improves the total radiation mechanism and the gain in the broadside direction. The major issue is that PMC structures do not exist in nature. Alternatively, to obtain PMC-like behavior, that is, 0° reflection characteristics, structures providing high surface impedance are desired. The fact is that high surface impedance makes the reflection coefficient $+1$, which can be understood using Equation (4) [14, 40].

$$\Gamma = \frac{Z_s - \eta_0}{Z_s + \eta_0} \tag{4}$$

where Γ = reflection coefficient on the surface due to normal incidence, Z_S = surface impedance, and η_0 = free-space impedance.

To meet high surface impedance, meta-material structures have been invented by arranging similar types of objects or metal periodically in 3-D, 2-D, and 1-D fashion [40], which is called metamaterial. However, 3-D meta materials such as photonic band-gap materials provide certain complexity in terms of design, placement, conformability, and size. On the other hand, 2-D metamaterials such as metasurface, where PEC is arranged over a 2-D dielectric substrate, are widely used in wearable applications due to their ease of design and compatibility [15–18]. There are many types of metasurface configurations, but the two most common are mushroom-like structures, which use metallic vias in between the periodic unit cells and ground plane as shown in Figure 4(a) and via-free metasurfaces, which do not use vias as shown in Figure 4(b). The use of metallic vias to produce a compact structure causes dissatisfaction in wearable applications and affects manufacturing. The absence of vias, on the other hand, enables simple fabrication, compatibility with common planar circuit technology, a low cost of manufacture, and a comfortable attachment to the body [40].

The following equations were developed by the authors of [14] and [40] to demonstrate the generation of a high sur-

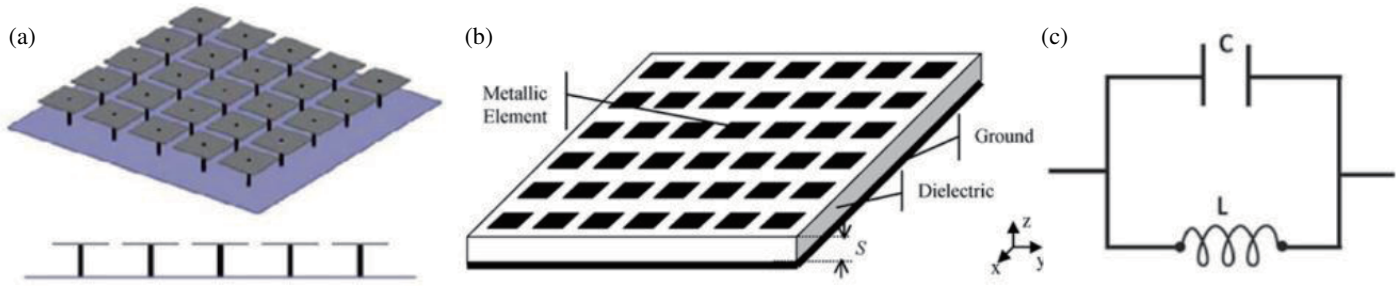

FIGURE 4. Structure of (a) Metasurface with via [14] (b) Metasurface without via [40], and (c) Equivalent-model.

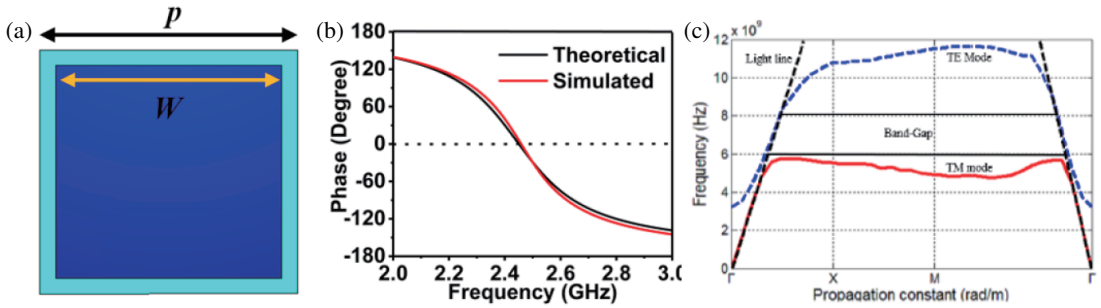

FIGURE 5. (a) Theoretically developed conventional unit-cell. (b) Theoretical and simulated reflection phase characteristic, and (b) Dispersive curves.

face impedance for a mushroom-type metasurface:

$$Z_s = \frac{jwL}{1 - w^2LC} \tag{5}$$

$$C = \frac{W\varepsilon_0(1+\varepsilon_r)}{\pi}\cosh^{-1}\left(\frac{W+g}{g}\right) \tag{6}$$

$$L = 2\times 10^{-7}h\left[\ln\left(\frac{2h}{r}\right) + 0.5\left(\frac{2r}{h}\right) - 0.75\right] \tag{7}$$

where C = grid capacitance generated by the gap between the unit-cell, L = inductance generated due to the current flowing in the metallic via, ε_0 = free space permittivity, ε_r = substrate's dielectric-constant, h = substrate's height, r = radius of the pin, W = unit-cell's width, and g = unit-cells gap. For high surface impedance, the circuit depicted in Figure 4(c) behaves as a parallel-resonant circuit, and the resonant frequency (f_r) and bandwidth (BW) are reproduced as follows:

$$f_r = \frac{1}{2\pi\sqrt{LC}} \tag{8}$$

$$BW = \frac{1}{\eta_0}\sqrt{\frac{L}{C}} \tag{9}$$

The researchers in [40] stated that the inductance can also be generated in the absence of metallic vias. The fact is that, when the metallic via between the patch and ground is not present, they act as a short-circuit transmission line for the substrate of less than a quarter-wave length thickness and generate an inductance L_d, also known as dielectric slab inductance, which can be represented as

$$L_d = \mu_0 h \tag{10}$$

where μ_0 = free space permeability.

5. PROPOSED THEORETICALLY DESIGN UNIT-CELL WITH ANALYSIS

Using the aforementioned equations, a conventional via-free rectangular unit-cell is theoretically designed at 2.45 GHz, as shown in Figure 5(a). Using Equation (10), inductance 'L_d' is estimated as 3.77 nH for 3 mm thicker substrate. The substrate is made of felt, which has $\varepsilon_r = 1.6$ and $\tan\delta = 0.044$. Cg is then determined to be 1.12 pF at 2.45 using Equation (8). Then, the unit-cell's size (W) is determined to be almost 35 mm, with the gap (g) being 1.5 mm using Equation (6). Using Equation (4), the theoretical reflection-phase characteristic is plotted and depicted Figure 5(b). Then, by designating the boundary as a unit-cell and the port as a Floquet port in CST Microwave Studio, the theoretically estimated unit-cell is simulated. The theoretically estimated reflection phase characteristic and the simulated reflection phase characteristic are both well-aligned as shown in Figure 5(b). The graphs convey that in the phase between $-90°$ to $+90°$, the surface impedance is greater than the air impedance and can be used for performance improvement. Nonetheless, the frequency-range for the phase variation $90° \pm 45°$ can only be used to improve performance [40]. The metasurfaces show a unique reflection phase characteristic of phases between $0°$ and $180°$, which is not possible in

the case of PEC, which reflects with a phase of 180° and PMC surface, which reflects with a phase of 0°. This type of metasurface is called artificial-magnetic-conductor (AMC) or high-impedance-surface (HIS).

The metasurface, which not only possesses 0° to 180° phase characteristics but also suppresses the surface wave for a particular range of frequency that is the surface wave band gap, is known as the electromagnetic band gap (EBG) [40]. The fact is that the presence of surface waves creates unwanted radiation, so waste of power occurs in the desired direction. Therefore, the surface wave needs to be suppressed to attain maximum radiation in the desired direction for the required frequency band. Equation (8) indicates a transverse magnetic (TM) wave of propagation for the frequency range below the resonance due to the inductive nature of the metasurface. At a higher frequency than the resonant frequency, the unit cells become capacitive and sustain the propagation of transverse electric (TE) waves. The TM and TE wave propagations are depicted in Figure 5(c) by a red solid line and a blue dashed line, respectively. The frequency ranges close to the resonance where the flow of TE and TM surface waves is blocked is referred to as the frequency band gap. These two characteristics, in-phase reflection characteristics and surface wave suppression, distinguish the metasurfaces-based antenna from conventional antennas and make it applicable to a wide variety of applications. The next section discusses the literature surveys on the advances in metasurface-inspired wearable antennas.

6. ADVANCEMENT IN METASURFACE-INSPIRED ANTENNAS

The major constraint that must be overcome while using an antenna near a human body is its high backward radiation. The high back radiation occurs due to the bidirectional nature of radiation of the antenna, which increases the SAR and creates unwanted body effects. To solve the aforementioned issues, metasurfaces based printed MAs have been mostly used in wearable applications, where the metasurfaces act like a reflector and minimize the backward radiation. In addition, the MAs provide wide impedance bandwidth, which helps in covering the required bands after the shifting of operating frequency bands due to bending and crumpling. The size of the antenna is another major constraint in the case of body-worn applications, because very little space is available for antenna placement due to the presence of other electronic gadgets. As a result, a smaller antenna is preferable in wearable applications. Additionally, a compact antenna can easily fit on the human body and can provide comfort compared to a larger size and provide less weight. Apart from the aforementioned features of the wearable antenna, there is also the need for circular polarization and dual-band operations. Because the human body is always in motion in realistic scenarios, the linear polarization of the emitted waves from the antenna might induce a polarization mismatch, resulting in an unsatisfactory wireless transmission. A circularly polarized wave, on the other hand, makes the signal more stable when the human body moves and is good for WBAN communication. Similarly, a dual-frequency band can reduce the complexity and cost of integration and increase the functionality of the devices more than a single-frequency band. Therefore, the surveys on metasurfaces-based MAs are divided into six categories: single band linearly polarized antenna; dual band linearly polarized antenna; single band circularly polarized antenna; dual band dual-polarized antenna; dual band dual-circularly polarized antenna; and dual band dual-polarized antenna. Each section discusses the techniques employed for common performance enhancements, including backward radiation minimization, SAR reduction, realized gain enhancement, radiation efficiency improvement, impedance bandwidth enhancement, and size reduction, as well as the obtained polarization and number of operating bands.

6.1. Single-Band Linearly Polarized Antenna

The authors of [41] have proposed the first metasurface-inspired antenna using an FR-4 substrate to attain the 2.45 GHz Industrial, Scientific, and Medical (ISM) bands. The metasurface reduced the amount of back-radiated wave and size with increased impedance BW and realized gain. The used substrate was rigid in nature and might cause problems during bending. After that, to provide flexibility, the authors of [42] invented an EBG-inspired wearable antenna using fabric substrates, which was later extended by the authors of [43]. In the mentioned literature, the presence of EBG improved the impedance bandwidth by 50% and reduced the size of the antenna by 30%. When EBG is present, the antenna works better than when EBG is not present.

With the growing popularity of EBG-based MA for a variety of wearable applications, the authors of [28] investigated a new form of antenna using flexible substrates. The design includes a 4×3 EBG-based printed MA, where the metasurface contains split ring resonator (SRR)-based unit-cell. Inkjet-printing methods are used to print the antenna on a paper substrate. To study the characteristics of metasurface, reflection phase characteristics have been explored. In addition, the authors investigated the impact on performance of raising the number and dimensions of unit-cells and repositioning themselves on the phantom. It was observed that the increase in size and number of unit cells enhanced performances. Furthermore, on the phantom, the EBG integrated antenna outperformed the antenna without EBG in terms of reflection coefficients, and an impedance bandwidth of 4.08% was achieved.

The authors of [33] have presented a coplanar waveguide (CPW)-fed M-shape printed monopole backed with Jerusalem Cross (JC) type unit-cell based AMC reflectors for the application of telemedicine at 2.45 GHz. The Jerusalem Cross shape of unit-cells was used not only to reduce backward radiation but also to provide miniaturization. The monopole radiators were fabricated using Kapton polyimide, and the AMC was fabricated using vinyl flexible substrates. To analyses the AMC characteristics, the reflection phase curves were presented. The presence of a metasurface reduces backward radiation, which aids in the improvement of impedance matching. As a result, the realized gain and front-to-back ratio (FBR) were enhanced by a 3 dB and 8 dB, respectively, with an impedance bandwidth of 18% and minimal frequency shifting near the human body. Furthermore, the SAR was reduced by 64% that

is, from 1.88 W/Kg when metasurfaces were not employed to 0.683 W/Kg with the integration of metasurfaces.

With the progress of inventing novel designs for backward radiation reduction, the researchers also focused on estimating the change in performance due to the unit-cell array size reduction [29]. The RT/Duroid 5880 dielectric was used as substrates for both metasurfaces and MA, which are semi-flexible in nature. To analyse the AMC characteristics, the reflection phase curves were presented. It was observed that the reduction of the unit-cell array from 4×3 to 2×1 still maintains the impedance bandwidth. The obtained realized gain, impedance bandwidth, and SAR are 6.88 dB, 5%, and 0.244 W/Kg, respectively, with a compact structure. The authors claim that the presented AMC integrated MA could be suitable for the use in biosensor or health monitoring applications.

In [33], the authors presented an EBG-based MA that operated at a frequency between 2.36 and 2.4 GHz. The unit-cells of the metasurface were of an I-shaped structure, acted as main radiators and also as ground planes. The presence of EBG improved the reflection coefficients with a fractional bandwidth of 5.5%, gain to 6.2 dB, FBR to more than 23 dB, and reduced the SAR by 95.3% compared to the MA in the absence of EBG. Furthermore, the authors found that, compared to conventional planar antennas such as quarter-wave length monopole and half-wave length microstrip, the metasurface-based antenna provided better performances during bending and human loading.

There is a growing interest in research on wrist-worn applications such as smartwatches. The antenna required to fit in smart watches must be flexible, highly directional, and compact with the features of low SAR. For better performance in smart watch communications, the authors of [44] reported an EBG inspired MA. The metasurface integrated antenna provided a directivity of 6.3 dB and an impedance bandwidth of 5.8%. The presence of EBG reduced the SAR from 13.5 W/Kg to 0.29 W/Kg.

In [7], an EBG-frequency selective surface (FSS) based MA was presented to attain 2.4 GHz medical body area network (MBAN) applications. Jeans substrate was used as a substrate. The presence of EBG-FSS beneath the MA reduced backward radiation that increased the gain to 6.55 dB and reduced the SAR by 95%. In addition, the authors compare the performance of EBG with the PEC by taking the same height and sizes. The result shows that the PEC reflectors have a poor reflection coefficient in the required bands below 10 dB and due to an 180° phase shift of reflected waves. In contrast, the presence of EBG-FSS provides a good reflection coefficient that is more than 10 dB in the required bands. Therefore, metasurfaces were becoming a more suitable choice than PEC reflectors.

In [30], the authors introduced a novel EBG-based 2.4 GHz antenna. The EBG structure is composed of 2×2 array of unit-cells, where each unit-cell contains a square loop and T-shaped strips. The MA has an E-shape like structure. To fabricate the antenna, the Shield It super-conductive textile conducting material is printed on a denim substrate. The presence of metasurface reduced the backward radiation, as a result of which the FBR was improved by 15.5 dB, realized gain enhanced to 7.8 dB, SAR reduced by 95%, and the impedance bandwidth enhanced to 27% with a reduction of frequency detuning. In advance of that, in [35], the authors introduced a textile-based AMC reflector at 2.4 GHz and analyzed the crumpling effects. The presence of AMC reduced the back-radiated waves that reduced the SAR by 90%. The authors of [21] then proposed a miniature EBG-based circular ring slot antenna operating at 2.4 GHz for wearable applications. A frequency BW of 360 MHz and a half power beamwidth (HPBW) of 60° in the H-plane and 54° in the E-plane were achieved. The presence of metasurface provided an FBR of 17 dB and 13 dB in the H- and E-planes, respectively with a very low SAR value.

In [36], the authors have presented an AMC based MA using Pellon as a dielectric and Pure Copper Taffeta as a conducting material to attain 5.8 GHz in the ISM band. The metasurface integrated antenna provides an impedance bandwidth of 34%, covering the 5.8 GHz ISM band with a peak realized gain of 6.12 dBi. The authors also analyzed the metasurface integrated antenna by bending, crumpling, and putting it on the human body, which shows better performance than an MA in the absence of metasurface. To conduct the on-body performance, different body models such as the cubic model, cylindrical model, and Ella model have been used along with phantom structures. Due to the presence of metasurface, safe values of SAR were obtained in every case.

After that, the authors of [37] have presented an EBG based MA to attain 2.4 GHz, where the unit-cell arrays are reduced from 3×4 to 2×3. The reduction of arrays did not affect the radiation performance and reduced the overall size by 50 %. The presence of metasurface increased the gain from 2.1 dB to 5.6 dB with the suppression of cross polarization. A very low value of 1 g and 10 g standard SAR values of 0.054 W/Kg and 0.0296 W/Kg, respectively, have been achieved due to the presence of metasurface. Then the same authors presented a metasurface based MA in [22] which was made of textile material to attain 5-GHz bands. The metasurfaces have been used to reduce backward radiation, and the PIFA is used to realize miniaturization. The metasurface integrated antenna covered the frequency range from 4.96 GHz to 5.90 GHz with a peak gain of 6.70 dB and a radiation efficiency of 77%. An oval-shaped printed MA backed by a 3×3 EBG structure to attain the 2.4 GHz ISM band was proposed in [24]. The authors' experiments showed that the MA, in the absence of EBG, provided satisfactory performance at a distance of 30 mm from the human body. In comparison, the presence of EBG improved the gain to 11.54 dB with a reduction of SAR of 99.5%. The authors of [45] then narrowed their focus to create a 2×2 AMC-based π-section MA with composite right/left handed (CRLH)-transmission-line-methodology at 2.4 GHz. The presence of AMC enhanced the free space gain by 5.29 dB, which is from 2.34 dB to 7.63 dB, and the free space radiation efficiency by 9.4%, which is from 87% to 96.4%. On the body, the gain was enhanced by 14.88 dB, and the radiation efficiency was enhanced by 72.4% with a very low value of SAR.

In addition to the above flexible dielectric and conducting materials, the authors of [46] have presented for the first time a metasurface-based MA with a liquid metal radiating element, such as EGaIn, and a soft and elastic Ecoflex 0030 substrate.

The presence of metasurface covered the 3.23 GHz to 3.59 GHz frequency range with a peak gain of 5.8 dB and a 1 g standard SAR of 1.25 W/Kg. To reduce the influence of the dense liquid's swinging, the ground plane was divided into six segments. In addition, as a result of the employment of pure water-resistant materials, a stable characteristic has been established in humid environments, making the antenna more suited for wearable applications.

A few articles, such as [47], [48], and [49], have introduced metasurfaces to enhance the propagation between two antennas present on the same body. Generally speaking, the transmission channels within the human body are vulnerable to fading or shading. Due to body motion, body structure, and local dispersion, on-body channels are subject to fluctuation. In addition, wearable antennas on the body have high propagation losses. Therefore, the transmission of information between antennas is crucial, especially in parts of the body with several devices. In contrast to antennas that radiate in empty space, antennas that are near the human body incur severe losses, which decrease their performance. To overcome these problems, the metasurface can be used as a jacket to improve the transmission efficiency between the antennas placed on it. The authors of [47] have placed the EBG structures in between two diamond-shaped dipole antennas with ports 1 and 2 assigned to them. It was observed that the presence of EBG enhanced the transmission quality, which was characterized by S_{21} curves between the two antennas. The coupling between the antennas was improved mainly due to the suppression of surface waves propagating between them. Further research [48, 49] on EBG demonstrates how it might enhance the transmission between antennas.

Apart from the above-mentioned applications, metasurfaces were also used in Radio Frequency Identification (RFID) applications to reduce the interference between the antenna and body [50, 51]. RFID is a contactless technique of identification that has been widely implemented in our lifestyles and industries, including the academia, healthcare, warehousing, aerospace, transportation, trading, and transportation sectors. In [50], the authors proposed a novel type of AMC to operate in the 868 MHz RFID band to solve the tag's proximity problem with metals and human tissue. The authors tested the fabricated antenna in an anechoic chamber by placing it on metallic objects and a human wrist. It was observed that the performances did not significantly change due to the presence of AMC. Then, the authors of [51] presented a belt-mounted 4×3 EBG-based MA for tracking human movements via communication between the proposed design and other electronic equipment. The metasurface integrated antenna was reported to function in the 2.45 GHz ISM band and produce a peak gain and SAR of 7.94 dB and 0.04 W/Kg, respectively.

[52] presents the first AMC-based Yagi-Uda antenna for improving end fire radiation using a Latex substrate for 2.4 GHz wireless communication applications. The utilization of the AMC metasurface converted the bidirectional end fire radiation of the Yagi-Uda antenna to an off-axis near-end fire radiation with a beam inclination of 74° toward the end fire direction. Single-layer and double-layer AMC surfaces with a 0° reflection phase are thought to reduce the amount of radiation absorbed by the body and, in turn, the peak specific absorption rate (SAR) level in the required frequency bands. The presence of a double layer metasurface enhanced the radiation efficiency to 78.97% and reduced the 10 g SAR to 0.7 W/Kg with an impedance BW and gain of 45 MHz and 0.12 dB, respectively.

6.2. Single-Band Circularly Polarized Antenna

To facilitate CP characteristics, the authors of [38] presented an anisotropic 2×2 EBG based MA to attain the 2.4 GHz ISM band. Metasurfaces were used to reduce back-radiation and to generate CP characteristics. The back-radiation was confirmed by the in-phase reflection-phase-characteristics. The polarization rotation characteristics were due to the truncating nature of unit-cells of the metasurface. To fabricate the integrated antenna, polydimethylsiloxane (PDMS) was used for the substrate, and silver nanowires (AgNWs) were used for the conducting materials. The presence of metasurface provided a gain of 5.2 dB, a 3-dB axial ratio (AR) BW of 69 MHz, and an FBR of 16 dB. Furthermore, the presence of metasurface provided stable performance due to deforming and human body loading. A very low SAR of 0.13 W/Kg under a 1 g standard was obtained.

After that, in [53], a 3×3 EBG based circularly polarized cross-dipole for RFID wearable application was proposed. The presence of EBG provided an impedance bandwidth of 3.2% with a gain improvement of 3.34 dB. Then in [52], a 2×2 AMC based printed MA was used to attain CP characteristics at 5.8 GHz. The CP characteristics were achieved by combining monopole feed and inverted L-shaped strips extended in one of the CPW ground planes. The presence of AMC provided the highest gain and radiation efficiency of 7.6 dB and 94.7%, respectively, with an SAR reduction of 20.42%. Then, in [55], a modified metasurface-based microstrip antenna for achieving wide AR-BW in the 5 GHz band was proposed. The antenna was constructed with a felt like substrate and nylon conducting material to provide flexibility. The metasurface integrated microstrip antenna had an impedance BW of 35.1%, an AR BW of 17.5%, a realized gain of 8.5 dB, and a SAR value that was extremely low. It was proposed that the antennas be used for both ON-body and OFF-body communications.

In [15, 16], we proposed metasurface-based circularly polarized antennas at 2.45 GHz. The circular polarization was generated using two distinct techniques. In the first case, a 45°-tilted monopole antenna was integrated onto a 3×3 anisotropic metasurface as shown in Figure 6 and the simulated results in Figure 7. The antenna produced an impedance BW, an AR BW, peak gain, and the highest efficiency of 330 MHz, 74 MHz, 6.6 dBi, and 69%, respectively, in free space (FS). Due to the presence of metasurface, the efficacy on the body is identical to that in FS with low SAR values.

As depicted in Figure 8, circular polarization is generated in the second instance by extending one of the ground planes in a vertical direction. To minimize backward radiation, AMC reflectors were utilized. The antenna is furnished with all characteristics in Stage 4 (S-4), which is followed by Stages 1, 2,

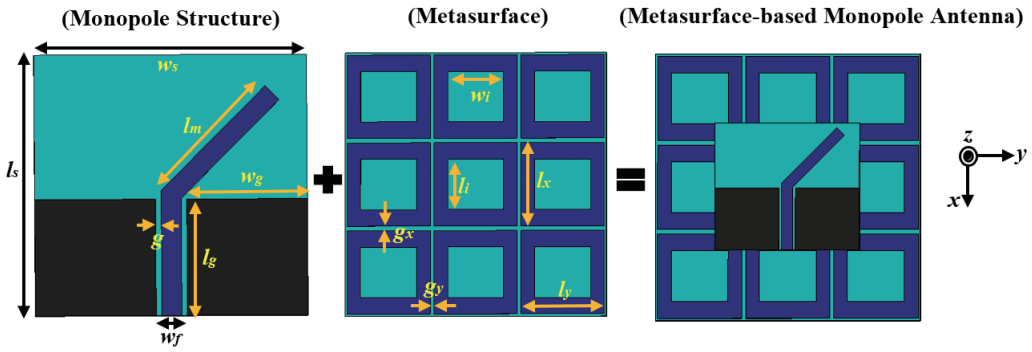

FIGURE 6. Metasurface based monopole antenna proposed in [15].

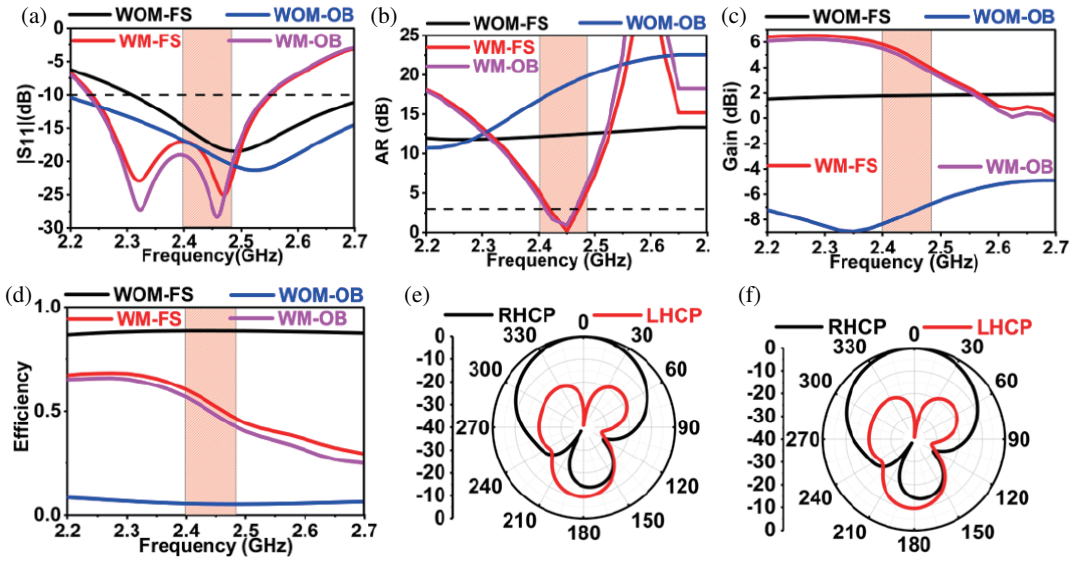

FIGURE 7. Antenna performances from [15] (a) S_{11}, (b) AR, (c) Gain, (d) Efficiency, (e) RHCP and LHCP Plots at 2.45 GHz in the xz-plane, and (f) RHCP and LHCP plots at 2.45 GHz in the yz-plane.

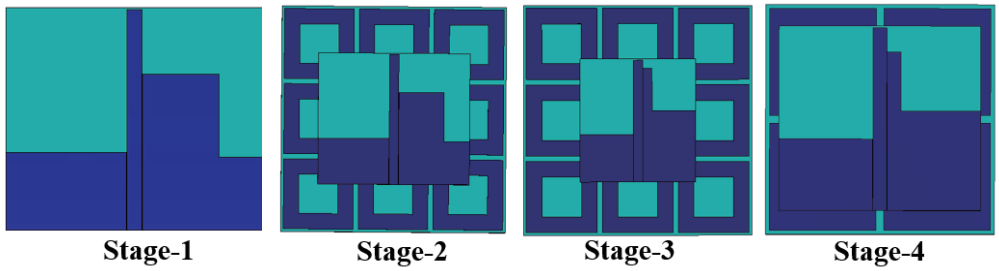

FIGURE 8. Evolution of proposed metasurface based monopole antenna of [16].

and 3 (S-1, S-2, and S-3). Due to its omnidirectional radiation patterns, S-1 initially performed inadequately in terms of impedance bandwidth, gain, radiation efficiency, and SAR on the body. On the other hand, by employing a 3×3 AMC in S-2, performance is enhanced. As the AR curve moved up, however, the monopole antenna was optimized in S-3, resulting in a further reduction in SAR and an increase in peak gain. Lastly, the 2×2 AMC in S-4 contributed to a 55.56% and 97.72% reduction in footprints and SAR, respectively. On the body, it provided 350 MHz impedance bandwidth, 67% radiation efficiency, 6.1 dBi peak gain, and 170 MHz 3-dB AR bandwidth, respectively. Figure 9 depicts the S-4 antenna, which has an impedance bandwidth of 580 MHz, a maximal gain of 6.5 dBi, and a 3 dB AR BW of 150 MHz. On the basis of the performance evolution from stage 1 to stage 4, it can be concluded that increasing the size of the reflector relative to the monopole antenna decreases SAR and increases peak gain.

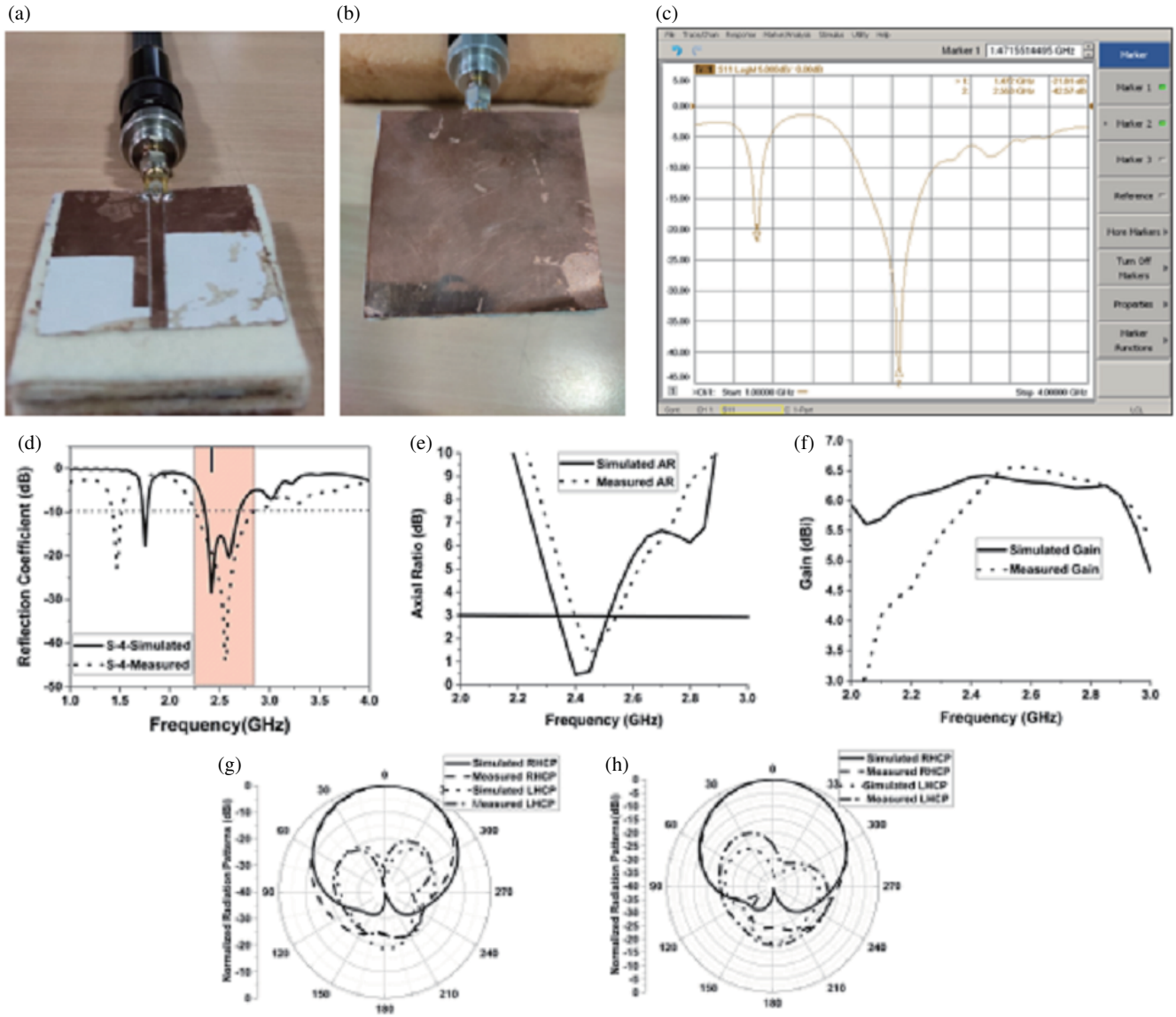

FIGURE 9. (a) Top view of fabricated antenna, (b) Back view of fabricated antenna, (c) S_{11} on VNA, (d) Measured S_{11}, (e) Measured AR, (f) Measured gain, (g) Measured RHCP and LHCP in xz-plane, and (h) Measured RHCP and LHCP in yz-plane [16].

6.3. Dual-Band Linearly Polarized Antenna

The authors of [30] have invented, for the first time, EBG using textile material. They proposed the work to achieve dual-band operation at 2.45 GHz and 5 GHz bands using coplanar printed monopole-based EBG structures. Dual-band operation is achieved by staking a dual-band MA on a dual-band EBG. The EBG was constructed using 3×3 arrays of conducting unit-cells on a felt substrate. It was observed that the presence of EBG reduced the backward radiation by 10 dB, which in turn enhanced the gain by 3 dB and reduced the SAR by a factor of 20. The authors also conducted the bending effect over the E-plane and H-plane, which showed unchanged impedance bandwidth in both cases. To conduct on-body performances, the metasurface integrated antenna was directly placed on the jeans of the thigh, the skin of the arm, and the cloth of the back side.

In [56], the authors investigated an MA backed by an AMC containing rectangular unit-cells to attain 2.4 GHz and 5 GHz in WLAN applications. The patch of the MA generated the lower frequency band, whereas a slot on it generated the upper frequency-band. To design the antennas, the radiators made of textile from the Shieldit TM Super family with a thickness of 0.17 mm were printed on 1.5 mm-thick felt substrates. In the given work, the presence of EBG improved the FBR by more than 12 dB in the required bands, with a maximum gain of 2.5 dB and 4 dB in the lower band and upper band, respectively. The authors also studied the bending performances with variant radii, which showed that the y-axis bending of the antenna changes significantly because of the change in the current distribution, while no changes occur in the case of x-axis bending because of no disturbance in the current distribution. It was reported that the lower frequency band shifted towards the

higher side while there was no shift in the higher band upon the decrement of the bending radius. To test the on-body performance, the EBG integrated antenna was positioned on the arm. The presence of metasurfaces had no effect on the performance of antennas while they were put on the body. Furthermore, the authors also studied the effect on SAR due to the increase in AMC size. The study showed that with the increase in unit-cell numbers, the SAR was reduced by a factor of greater than 10.

Another dual-band antenna was presented in [56] using a fractal-based MA backed by an EBG structure. The antenna was proposed to attain the 1.8 GHz GSM band and 2.45 GHz ISM bands. Dual-band operation was achieved due to the fractal nature of the printed MA. A dielectric material of 1 mm thick was chosen as the substrate. The presence of EBG retained the overall performance of the human body as if it were in free space. In addition, the authors also conducted the bending and crumpling analysis, which showed that the presence of EBG forced the antenna to operate in the required bands without any frequency shifting. Also, the presence of EBG reduces backward radiation by more than 15 dB, which helps bring the SAR down to safe levels and boosts the gain. After that, to provide miniaturization, the authors of [58] proposed a metamaterial-loaded antenna using CRLH transmission line theory for operating in the 2.4 GHz and 5.2 GHz frequency bands in WLAN applications. The first-order positive (that is, $n = +1$) and negative (that is, $n = -1$) modes were excited to obtain similar kinds of radiation patterns in both the bands. A very low level of backward radiation was obtained, which in turn reduces the SAR to safe values.

In [32], the authors have suggested a 3×3 AMC based U-shaped MA. The adjusting of the folding of the U-shape of the MA generated dual band operations at 2.4 GHz and 5.8 GHz. To provide flexibility, the antenna was fabricated using a polyimide substrate. The presence of EBG increased the on-body gain by 9.3 dB in the lower band and 5.37 dB in the higher band, and the radiation efficiency by 48.4% in the lower band and 35.70% in the higher bands. Furthermore, due to backward radiation minimization, the SAR was reduced by more than 70% in both the bands. The authors of [59] then achieved dual-band operation at 2.4 GHz and 3.5 GHz, using a triangular slotted printed MA fabricated on a Rogers ULTRALAM 3850 substrate, and backward radiation reduction using an AMC containing 4×4 arrays of unit-cell on an RO3003 substrate. The backward radiation reduction of the metasurfaces enhanced the free space gain by 6.8 dB in the lower band and 3.7 dB in the higher band. On the body, these gains are enhanced by 23.3 dB and 13.9 dB with a SAR reduction of 99% in both bands. Therefore, the authors have recommended using the antennas for diabetic patients.

To enhance the functionality of the metasurface, that is, to reduce the backward radiation also for dual band frequency generation, the authors of [60] and [6] have proposed dual mode metasurfaces. In [60], the metasurface was operated in TM_{11} mode at 2.45 GHz and TM_{02} mode at 5 GHz. The TM_{11} mode generated broadside radiation patterns which could be used in OFF-body communication, whereas the TM_{02} mode generated omnidirectional radiation patterns which could be used in ON-body communication. Both the radiating patch, which is the circular patch antenna, and the metasurface were fabricated using a PDMS substrate to provide flexibility in wearable applications. The authors used a bottom feed technique to feed the antenna. An impedance bandwidth of 4.9% with a gain of 5.5 dB in the lower band and an impedance bandwidth of 15.7% with a gain of 5.3 dBi were achieved by the metasurface based antenna. Furthermore, the resultant SARs in both the bands came below the safe value, which made them great candidates in wearable applications. In advance of [60], the authors of [6] have approached the CRLH transmission line theory to design the metasurface to obtain compactness. The metasurface is operated in the first negative mode, that is $n = -1$ at 2.45 GHz, and the first positive mode, that is $n = +1$ at 3.65 GHz, to generate broad side radiation patterns in both the bands. The excitation of this metasurface by a CPW-fed circular patch antenna generated a dual frequency of operations. The modes of the metasurface were analyzed using a dispersion curve. A peak gain of 4.25 dB in the lower band and 7.35 dB in the upper band was achieved. The ON-body implementation of the metasurface based antenna resulted in a very low SAR value in both bands, which makes it a suitable candidate for WBAN applications. After that, the same authors extended their work to design a novel 4×4 metasurface to attain 2.45 GHz band and 5.5 GHz band. The dual mode operation, that is, the -2nd ($n = -2$) mode and the $+1$st ($n = +1$) mode, generates dual frequency bands with unidirectional radiation patterns. The antenna provided an impedance bandwidth of 10.2% with a peak gain of -0.67 dB and an impedance bandwidth of 22.5% with a peak gain of 7.4 dB in the higher band. The backward radiation minimization lowered the SAR to below the safe value, which makes it a suitable candidate for wearable application.

6.4. Dual-Band Dual Polarized Antenna

A very few researchers, such as the authors of [61], have focused their research on developing dual-band dual-polarized metasurface based antennas in the field of WBAN to achieve dual band operations with circular polarization characteristics in one band and linear polarization characteristics in other bands. The design was presented to achieve circular polarization at 1.575 GHz bands and 2.45 GHz bands. The metasurface was designed to reduce backward radiation and fabricated by etching a 3×3 array of ShieldIt Super conducting material on a fully ground-backed felt substrate. A square ring in the center and square slits on the center of each side were introduced on a conventional rectangular patch to design the individual unit-cell of the metasurface. On the other hand, the top radiator, which is a square patch, was truncated at the corners of one diagonal to generate dual-band operations, and a rectangular slit was introduced on each corner of the truncated patch to generate circular polarization. The substrate was made of Kevlar. The metasurface integrated antenna provided an impedance BW, peak gain, AR BW, FBR, efficiency, and SAR of 7.6%, 1.98 dBi, 10%, 16.7 dB, 73.6%, and 0.78 W/Kg, respectively, in the lower band (LB). In the high band (LB), impedance BW, peak gain, AR BW, FBR, efficiency, and SAR are 5.5%, 1.94 dB, 12 dB, 83.3%, and 0.71 W/Kg, respectively.

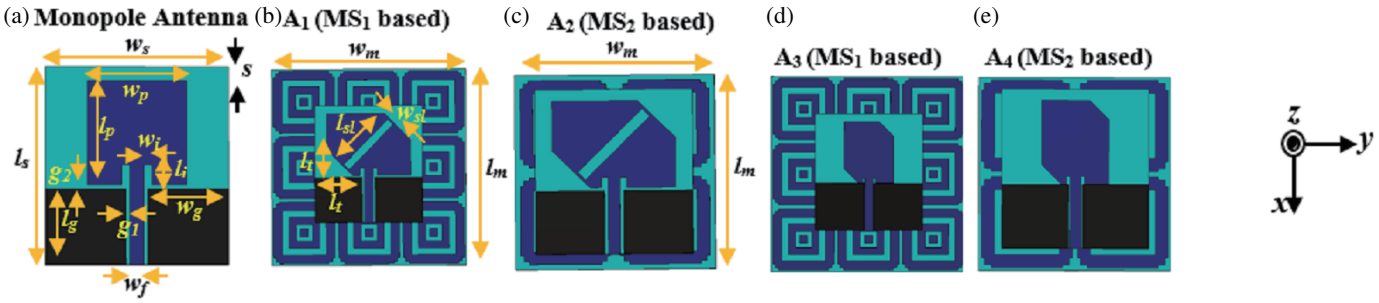

FIGURE 10. Structure of (a) Square monopole, (b) A_1, (c) A_2, (d) A_3, and (e) A_4 of [17].

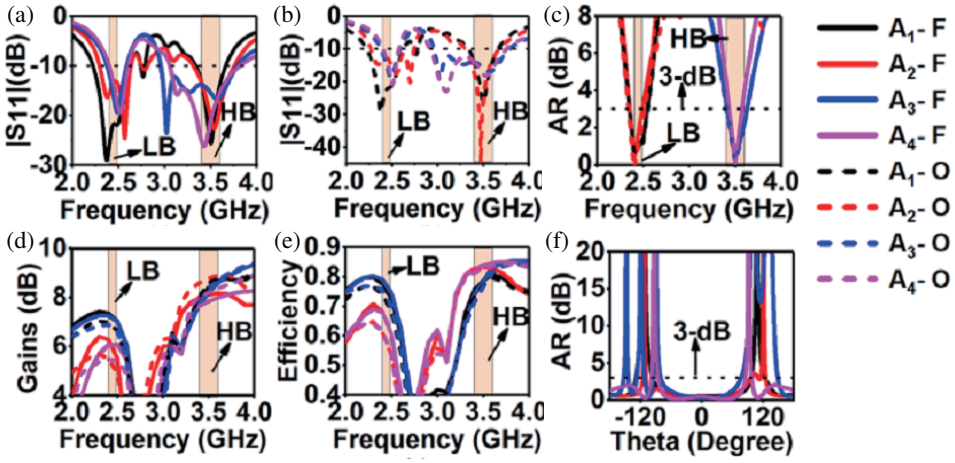

FIGURE 11. Simulated antenna performances (a) FS reflection coefficients, (b) OB reflection coefficients, (c) FS and OB AR, (d) FS and OB Gain, (e) FS and OB Radiation Efficiencies, and (f) AR Vs. theta curves of A_1 and A_2 at 2.4 GHz, and A_3 and A_4 at 3.5 GHz of [17].

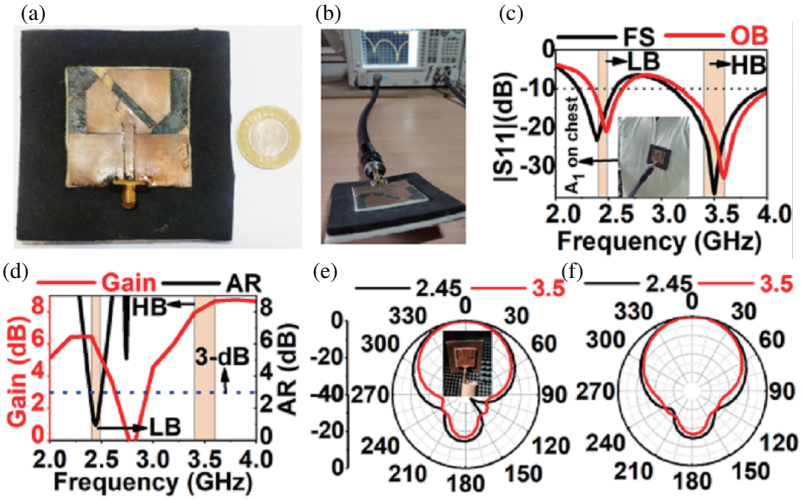

FIGURE 12. Fabricated structure of A1, (b) Set-up for measurement of FS reflection coefficient using VNA, (c) Measured FS and OB reflection coefficients, (d) Measured FS gain and AR, (e) Measured FS radiation patterns in xz-plane, and (f) Measured FS radiation patterns in yz-plane of [17].

We developed metasurface-based truncated monopole antennas as shown in Figure 10 to generate dual-band with dual-polarizations and reported in [17]. Metasurface was utilized not just for back-radiation lowering but also for dual-band generation, and a truncated monopole was utilized to attain CP characteristics. The metasurface is operated in TM_{10} and TM_{20} modes, which produce dual-band signals at 2.45 and 3.5 GHz bands, respectively. Using a transmission-line model and dispersion curve, two distinct unit-cells, UC_1 and UC_2, are optimized for the construction of 3×3 (MS_1) and 2×2 (MS_2) metasurfaces, respectively. Then, four variant truncated monopole structures stimulate these metasurfaces to design four dual-

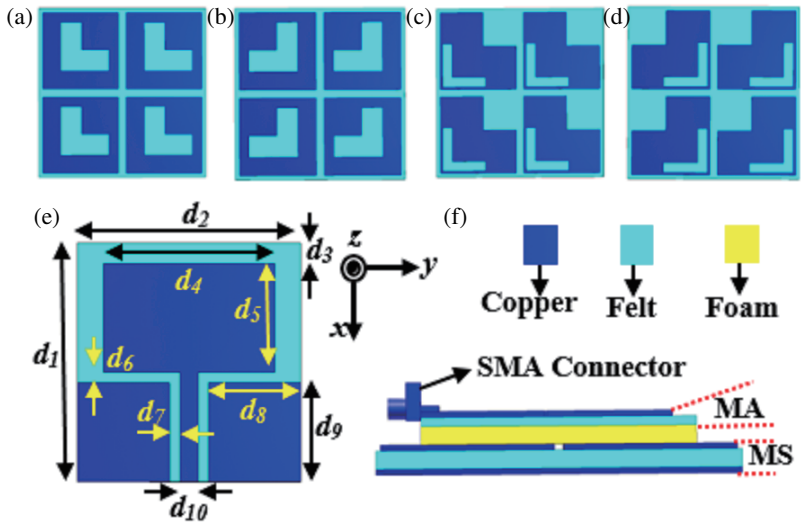

FIGURE 13. Structure of (a) MS_1, (b) MS_2, (c) MS_3, (d) MS_4, (e) MA, and (f) MS based MA [18].

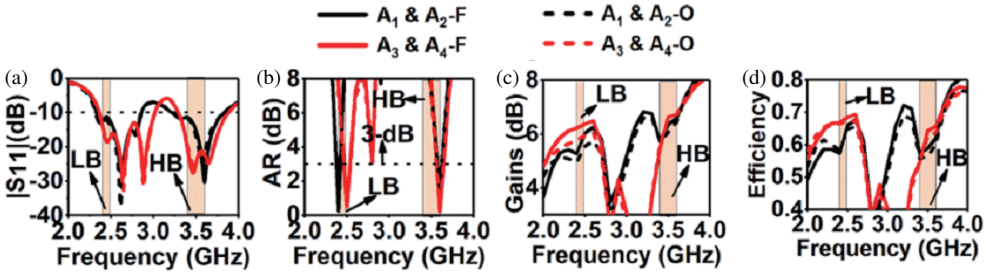

FIGURE 14. Simulated Free Space (F) and On-body (O) Performances (a) S_{11}, (b) AR, (c) Gain, and (d) Efficiencies of antennas [18].

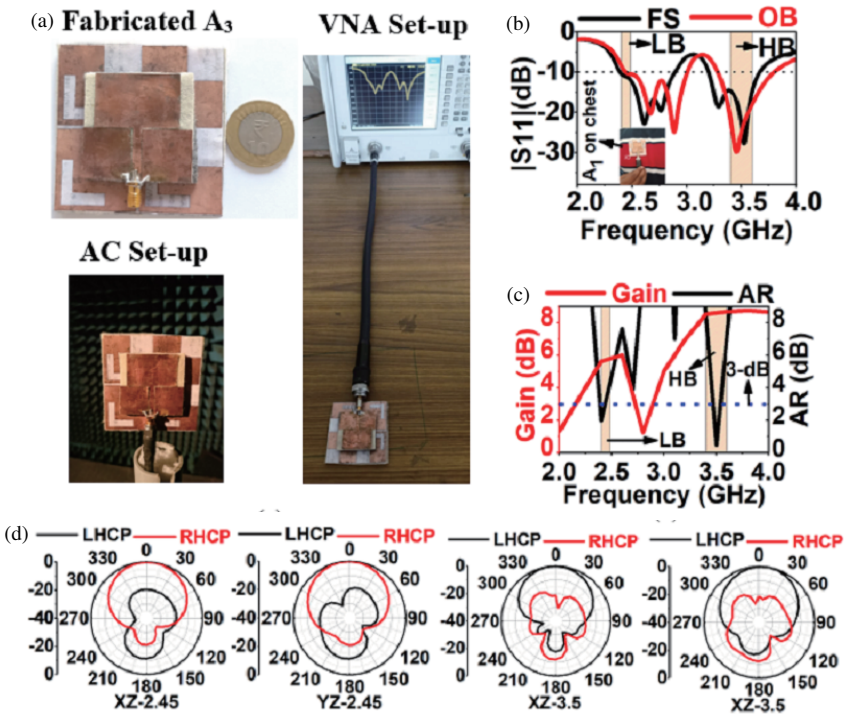

FIGURE 15. (a) The schematic of the fabricated A_3, S_{11}, Measurement set-up using the VNA and radiation pattern measurement set-up inside the anechoic chamber (AC), (b) Measured FS and OB S_{11} with OB measurement set-up in the insert, (c) Measured FS gain and AR, (d) Measured FS LHCP and RHCP at 2.45 GHz and 3.5 GHz in the xz and yz-planes [18].

TABLE 3. Performance comparison of existing literature.

Ref.	Freq. (GHz)	BW(%)	Gain (dB)	SAR (W/Kg)	Use of Metasurface	Polarization	Reason of Dual-band	Reason of CP
[32]	2.45	4.44	6.01	0.44	BRM	LP	-	-
[23]	2.45	6.3	4.077	0.09	BRM	LP	-	-
[24]	2.45	15.7	2.45	0.007	BRM	LP	-	-
[37]	2.48	3.4	5.6	0.02	BRM	LP	-	-
[35]	2.45	16.6	8.55	0.136	BRM	LP	-	-
[38]	2.4	10.7	5.2	-	BRM	RHCP	Anisotropic AMC	-
[16]	2.45	11.11	6.1	0.06	BRM	RHCP	Extended Coplanar Ground	-
[59]	3.5/5.8	5/7.4	9.07/7.66	0.136/0.66	BRM	LP/LP	Triangular-slotted-MA	-
[56]	2.45/5.5	12/16.3	2.5/0~4	0.019/0.009	BRM	LP/LP	Patch on MA for LB and Slot on it for HB	-
[31]	2.45/5.8	4/12	6.4/7.6	0.08/0.18	BRM	LP/LP	Dual-band MA	-
[57]	1.8/2.45	10.9/5.1	1~2	0.048/0.032	BRM	LP/LP	Fractal Nature of MA	-
[6]	2.45/3.65	15.7/2.3	4.25/7.35	0.65/0.37	BRM & DBG	LP/LP	EDM	-
[17] (A1)	2.45/3.5	17/9.5	7.4/8.8	0.02/0.02	BRM & DBG	CP/LP	EDM	Truncation on MA
[17] (A2)	2.45/3.5	14.3/12.8	6.4/8.2	0.09/0.03	BRM & DBG	CP/LP	EDM	Truncation on MA
[17] (A3)	2.45/3.5	8.9/25.2	7.3/9	0.02/0.02	BRM & DBG	LP/CP	EDM	Truncation on MA
[17] (A4)	2.45/3.5	8.5/23.8	6.1/8.3	0.07/0.03	BRM & DBG	LP/CP	EDM	Truncation on MA
[20] (P-I)	3.5/5.8	11.7/9.1	6.6/7.2	0.29/0.15	BRM & DBG & CPG	LHCP/RHCP	EDM	PCMS
[20] (P-II)	3.5/5.8	11.7/7.2	5.9/6	0.128/0.043	BRM & DBG & CPG	LHCP/LHCP	EDM	PCMS
[18] (A1)	2.45/3.5	20.5/17.7	6.3/7.9	0.06/0.1	BRM & DBG & CPG	LHCP/LHCP	EDM	PCMS
[18] (A2)	2.45/3.5	20.5/17.7	6.3/7.9	0.06/0.1	BRM & DBG & CPG	RHCP/RHCP	EDM	PCMS
[18] (A3)	2.45/3.5	24/16.8	6.5/7.8	0.04/0.06	BRM & DBG & CPG	RHCP/LHCP	EDM	PCMS
[18] (A4)	2.45/3.5	24/16.8	6.5/7.8	0.04/0.06	BRM & DBG & CPG	LHCP/RHCP	EDM	PCMS

BRM: Back radiation minimization, EDM: Excitation of Dual-mode, and DBG-Dual band generation.

band dual-polarized antennas (A_1, A_2, A_3, and A_4). Figure 11 demonstrates that A_1 and A_2 generate a 3-dB AR BW of 210 and 160 MHz in the LB, while A_3 and A_4 generate 230 and 170 MHz in the higher band (HB). MS_1-based antennas exhibit a peak gain of approximately 7.5 dBi in the LB and 9 dBi in the HB, with greater than 80% radiation efficiency in desired-bands, while MS_2-based antennas exhibit a peak gain of approximately 6.5 dBi in the LB and 8.3 dBi in the HB, with greater than 70% radiation efficiency in desired-bands. MS_2-based antennas, on the other hand, have a 52% smaller footprint than MS_1-based antenna. Figure 12 depicts the fabrication and measurement of A_1, which exhibits outstanding agreement with simulations.

6.5. Dual-Band Dual Circularly Polarized Antenna

Recently, the authors of [20] have presented a metasurface based MA to attain circular polarization in dual bands, that is, at 3.5 GHz for WiMAX and 5.8 GHz for ISM bands. The metasurface not only reduced the backward radiation but also generated circular polarizations in both the bands. A polarization converting metasurface was used, which when being incident by a linearly polarized wave from a dual-band MA, converts it to an orthogonally polarized wave. The polarization mechanism was understood with the help of dyadic reflection curves. The left-handed circular polarization (LHCP) and right-handed circular polarization (RHCP) states of polarization were conformed in the lower band and higher band, respectively. The

metasurface integrated antenna provided an impedance BW, AR-BW, efficiency, gain, and SAR of 11.7%, 2%, 47%, 6.6 dB, and 0.01 W/Kg, respectively in the LB. In the HB, the outcomes were 9.1%, 8.20%, 50%, 7.2 dB, and 0.043 for impedance BW, the AR BW, efficiency, gain, and SAR, respectively.

To accomplish dual-bands with dual circular polarizations, we developed polarization converting metasurface (PCMS)-based MAs [18], as depicted in Figure 13. The metasurface is used to reduce back-radiation and generate dual-bands at 2.45 GHz and 3.5 GHz with CP characteristics. The desired behavior is attained with the incident x-polarized wave on the PCMS coming from the monopole antenna (MA), t The PCMS works in TM_{10} and TM_{20} modes which produce dual frequency bands and reflect a 90°-phase-shifted y-polarized wave that, when combined with the 0°-phased x-polarized wave, generates CP. To achieve four separate configurations of phase-shift in terms of $+90°$ and $-90°$ in dual-bands, four distinct 2×2 PCMSs, designated as MS_1, MS_2, MS_3, and MS_4, are designed. In both frequency bands, the MS_1-based MA (A_1) generates LHCP, while the MS_2-based MA (A_2) generates RHCP. MS_3-based MA (A_3) produces RHCP in the LB and LHCP in the HB, while MS_4-based MA (A_4) produces LHCP in the LB and RHCP in the HB. Figure 14 illustrates the simulated free-space and OB antenna performances. Each antenna has a wide impedance BW, high gain, high efficiency, and low value of SAR. The fabricated structures of A_3 with measured results are depicted in Figure 15. The measured results were in good agreement with the simulation ones. A summary of frequency band, BW, gain, SAR distribution, use of metasurface state of polarization, reason for dual-band generation, and reason for CP generation by the literature is included in Table 3.

7. CONCLUSION

In this paper, the advances in the use of metasurfaces in wearable antenna design for off-body communications are presented. Initially, the design of the wearable antenna is discussed along with the summarization of the used material with dielectric properties by the researchers. Then the theoretical perspective on performance enhancements is discussed in depth. Using the discussed theories, a unit cell of the metasurface is designed theoretically and analyzed using CST Microwave Studio. The simulated and theoretical designs agreed well with each other. Following that, the advances of metasurfaces in terms of outcomes that include single-band with LP, single-band with CP, dual-band with LP, dual-band with dual-polarization, and dual-band with dual CP are discussed. At the end of the surveys, a comprehensive comparison table that includes operating frequencies, impedance bandwidth, gain, SAR, the use of metasurface, polarization, the reason for dual-band generation, and the reason for CP characteristics has been assembled to highlight the research's advancements. The literature survey conveys that most of the research in wearable applications has concentrated on the development of single-band linearly polarized metasurface-based monopole antennas. Few studies have been conducted on developing single-band circularly polarized metasurface-based monopole antennas. Dual-band dual-polarized metasurface-based monopole antennas and dual-band dual-circularly polarized metasurface-based monopole antennas are, nevertheless, quite rare at this time. In addition, the researchers have utilized metasurface solely as reflectors that reduce backward radiation only, and the utilization of metasurface for the generation of dual-band and circular polarization is very rare. The use of metasurfaces in wearable applications has resolved a number of issues that are not possible using conventional antennas.

REFERENCES

[1] Hall, P. S. and Y. Hao, *Antennas and Propagation For Body-centric Wireless Communications*, Artech House, Noorwood, MA, USA, 2012.

[2] Naik, N. C., N. K. Sahu, B. K. Ekka, and T. K. Patra, "Performance improvement of antenna using metasurface: An overview," *Progress In Electromagnetic Research B*, Vol. 101, No. 3, 63–64, 2023.

[3] Sahu, N. K., N. C. Naik, B. R. Behera, M. C. Tripathy, and S. K. Mishra, "Polarization converting metasurface inspired circularly-polarized antenna for OFF body communications," in *2023 1st International Conference on Circuits, Power and Intelligent Systems (CCPIS)*, 1–5, Bhubaneswar, India, 2023.

[4] Naik, N. C., N. K. Sahu, and T. K. Patra, "Compact metasurface-based dual-band antenna for off-body communications," in *2023 1st International Conference on Circuits, Power and Intelligent Systems (CCPIS)*, 1–5, Bhubaneswar, India, 2023.

[5] Naik, N. C., N. K. Sahu, and T. K. Patra, "Performance analysis of different shape CSRR antenna at 2.4 GHz," in *Proc. of the Int. Conf. on Advances in Comm. Engg.*, 1–5, 2023.

[6] Zhang, K., G. A. E. Vandenbosch, and S. Yan, "A novel design approach for compact wearable antennas based on metasurfaces," *IEEE Transactions on Biomedical Circuits and Systems*, Vol. 14, No. 4, 918–927, Aug. 2020.

[7] Ashyap, A. Y. I., S. H. B. Dahlan, Z. Z. Abidin, M. I. Abbasi, M. R. Kamarudin, H. A. Majid, M. H. Dahri, M. H. Jamaluddin, and A. Alomainy, "An overview of electromagnetic band-gap integrated wearable antennas," *IEEE Access*, Vol. 8, 7641–7658, 2020.

[8] Liu, H., P. Wen, S. Zhu, B. Ren, X. Guan, and H. Yu, "Quad-band CPW-fed monopole antenna based on flexible pentangle-loop radiator," *IEEE Antennas and Wireless Propagation Letters*, Vol. 14, 1373–1376, 2015.

[9] Agneessens, S., S. Lemey, T. Vervust, and H. Rogier, "Wearable, small, and robust: The circular quarter-mode textile antenna," *IEEE Antennas and Wireless Propagation Letters*, Vol. 14, 1482–1485, 2015.

[10] Liu, L., S. Zhu, and R. Langley, "Dual-band triangular patch antenna with modified ground plane," *Electronics Letters*, Vol. 43, No. 3, 140–141, Feb. 2007.

[11] Hertleer, C., H. Rogier, L. Vallozzi, and L. V. Langenhove, "A textile antenna for off-body communication integrated into protective clothing for firefighters," *IEEE Transactions on Antennas and Propagation*, Vol. 57, No. 4, 919–925, Apr. 2009.

[12] Sahu, N. K. and S. K. Mishra, "Cavity model analysis of dual polarized microstrip antennas for wireless body area network application," *International Journal of System Assurance Engineering and Management*, Vol. 14, 635–642, May 2023.

[13] Ullah, U., I. B. Mabrouk, and S. Koziel, "A compact circularly polarized antenna with directional pattern for wearable off-body communications," *IEEE Antennas and Wireless Propagation Letters*, Vol. 18, No. 12, 2523–2527, Dec. 2019.

[14] Sievenpiper, D., L. J. Zhang, R. F. J. Broas, N. G. Alexópolous, and E. Yablonovitch, "High-impedance electromagnetic surfaces with a forbidden frequency band," *IEEE Transactions on Microwave Theory and Techniques*, Vol. 47, No. 11, 2059–2074, Nov. 1999.

[15] Sahu, N. K. and S. K. Mishra, "Anisotropic metasurface inspired circularly-polarized monopole antenna for off body communications," in *2022 IEEE Wireless Antenna and Microwave Symposium (WAMS 2022)*, Jun. 2022.

[16] Sahu, N. K. and S. K. Mishra, "A compact low SAR and high gain circularly polarized AMC integrated monopole antenna for WBAN applications," *Progress In Electromagnetics Research C*, Vol. 113, 211–226, 2021.

[17] Sahu, N. K. and S. K. Mishra, "Compact dual-band dual-polarized monopole antennas using via-free metasurfaces for off-body communications," *IEEE Antennas and Wireless Propagation Letters*, Vol. 21, No. 7, 1358–1362, 2022.

[18] Sahu, N. K. and S. K. Mishra, "Polarization converting metasurface inspired monopole antenna for off-body communication," *IEEE Antennas Wireless Propag. Lett.*, Vol. 22, No. 1, 194–198, 2023.

[19] Das, S., A. Rajput, and B. Mukherjee, "A novel FSS based band stop filter for TE/TM polarization," *IEEE Letters on Electromagnetic Compatibility Practice and Applications*, 2023.

[20] Yang, H., X. Liu, Y. Fan, and L. Xiong, "Dual-band textile antenna with dual circular polarizations using polarization rotation AMC for off-body communications," *IEEE Transactions on Antennas and Propagation*, Vol. 70, No. 6, 4189–4199, Jun. 2022.

[21] Gao, G.-P., B. Hu, S.-F. Wang, and C. Yang, "Wearable circular ring slot antenna with EBG structure for wireless body area network," *IEEE Antennas and Wireless Propagation Letters*, Vol. 17, No. 3, 434–437, Mar. 2018.

[22] Gao, G.-P., C. Yang, B. Hu, R.-F. Zhang, and S.-F. Wang, "A wearable PIFA with an all-textile metasurface for 5 GHz WBAN applications," *IEEE Antennas and Wireless Propagation Letters*, Vol. 18, No. 2, 288–292, Feb. 2019.

[23] Yan, S. and G. A. E. Vandenbosch, "Radiation pattern-reconfigurable wearable antenna based on metamaterial structure," *IEEE Antennas and Wireless Propagation Letters*, Vol. 15, 1715–1718, 2016.

[24] El Atrash, M., O. F. Abdalgalil, I. S. Mahmoud, M. A. Abdalla, and S. R. Zahran, "Wearable high gain low SAR antenna loaded with backed all-textile EBG for WBAN applications," *IET Microwaves Antennas & Propagation*, Vol. 14, No. 8, 791–799, Jul. 2020.

[25] Jiang, Z. H. and D. H. Werner, "Robust low-profile metasurface-enabled wearable antennas for off-body communications," in *2014 8th European Conference on Antennas and Propagation (EuCAP)*, 21–24, Hague, Netherlands, Apr. 2014.

[26] Ouyang, Y. and W. J. Chappell, "High frequency properties of electro-textiles for wearable antenna applications," *IEEE Transactions on Antennas and Propagation*, Vol. 56, No. 2, 381–389, Feb. 2008.

[27] Ullah, M. A., M. T. Islam, T. Alam, and F. B. Ashraf, "Paper-based flexible antenna for wearable telemedicine applications at 2.4 GHz ISM band," *Sensors*, Vol. 18, No. 12, 4214, Dec. 2018.

[28] Kim, S., Y.-J. Ren, H. Lee, A. Rida, S. Nikolaou, and M. M. Tentzeris, "Monopole antenna with inkjet-printed EBG array on paper substrate for wearable applications," *IEEE Antennas and Wireless Propagation Letters*, Vol. 11, 663–666, 2012.

[29] Abbasi, M. A. B., S. S. Nikolaou, M. A. Antoniades, M. N. Stevanovic, and P. Vryonides, "Compact EBG-backed planar monopole for BAN wearable applications," *IEEE Transactions on Antennas and Propagation*, Vol. 65, No. 2, 453–463, Feb. 2017.

[30] Ashyap, A. Y. I., Z. Z. Abidin, S. H. Dahlan, H. A. Majid, S. M. Shah, M. R. Kamarudin, and A. Alomainy, "Compact and low-profile textile EBG-based antenna for wearable medical applications," *IEEE Antennas and Wireless Propagation Letters*, Vol. 16, 2550–2553, 2017.

[31] Zhu, S. and R. Langley, "Dual-band wearable textile antenna on an EBG substrate," *IEEE Transactions on Antennas and Propagation*, Vol. 57, No. 4, 926–935, Apr. 2009.

[32] Wang, M., Z. Yang, J. Wu, J. Bao, J. Liu, L. Cai, T. Dang, H. Zheng, and E. Li, "Investigation of SAR reduction using flexible antenna with metamaterial structure in wireless body area network," *IEEE Transactions on Antennas and Propagation*, Vol. 66, No. 6, 3076–3086, Jun. 2018.

[33] Raad, H. R., A. I. Abbosh, H. M. Al-Rizzo, and D. G. Rucker, "Flexible and compact AMC based antenna for telemedicine applications," *IEEE Transactions on Antennas and Propagation*, Vol. 61, No. 2, 524–531, Feb. 2013.

[34] Jiang, Z. H., D. E. Brocker, P. E. Sieber, and D. H. Werner, "A compact, low-profile metasurface-enabled antenna for wearable medical body-area network devices," *IEEE Transactions on Antennas and Propagation*, Vol. 62, No. 8, 4021–4030, Aug. 2014.

[35] Alemaryeen, A. and S. Noghanian, "Crumpling effects and specific absorptions rate of flexible AMC integrated antennas," *IET Microwaves Antennas & Propagation*, Vol. 12, No. 4, 627–635, Mar. 2018.

[36] Alemaryeen, A. and S. Noghanian, "On-body low-profile textile antenna with artificial magnetic conductor," *IEEE Transactions on Antennas and Propagation*, Vol. 67, No. 6, 3649–3656, Jun. 2019.

[37] Gao, G., R. Zhang, C. Yang, H. Meng, W. Geng, and B. Hu, "Microstrip monopole antenna with a novel UC-EBG for 2.4 GHz WBAN applications," *IET Microwaves Antennas & Propagation*, Vol. 13, No. 13, 2319–2323, Oct. 2019.

[38] Jiang, Z. H., Z. Cui, T. Yue, Y. Zhu, and D. H. Werner, "Compact, highly efficient, and fully flexible circularly polarized antenna enabled by silver nanowires for wireless body-area networks," *IEEE Transactions on Biomedical Circuits and Systems*, Vol. 11, No. 4, 920–932, Aug. 2017.

[39] Belrhiti, L., F. Riouch, A. Tribak, J. Terhzaz, and A. M. Sanchez, "Flexible antennas design and test for human body applications scenarios," *Microwaves, Optoelectron. Electromagn. Appl.*, Vol. 16, No. 2, 494–513, 2017.

[40] Goussetis, G., A. P. Feresidis, and J. C. Vardaxoglou, "Tailoring the AMC and EBG characteristics of periodic metallic arrays printed on grounded dielectric substrate," *IEEE Transactions on Antennas and Propagation*, Vol. 54, No. 1, 82–89, 2006.

[41] Salonen, P., M. Keskilammi, and L. Sydänheimo, "A low-cost 2.45 GHz photonic band-gap patch antenna for wearable systems," in *11th International Conference on Antennas and Propagation (ICAP 2001)*, Vol. 2001, No. 480, 719–723, Univ. Manchester, Inst. Sci. & Technol., Apr. 2001.

[42] Salonen, P., F. Yang, Y. Rahmat-Samii, and M. Kivikoski, "WEBGA — wearable electromagnetic band-gap antenna," in *IEEE Antennas and Propagation Society Symposium*, Vol. 1, 451–454, Monterey, Ca, Jun. 2004.

[43] Tsolis, A., W. G. Whittow, A. A. Alexandridis, and J. C. Vardaxoglou, "Embroidery and related manufacturing techniques for wearable antennas: challenges and opportunities," *Electronics*, Vol. 3, No. 2, 314–338, 2014.

[44] Chen, Y.-S. and T.-Y. Ku, "A low-profile wearable antenna using a miniature high impedance surface for smartwatch ap-

plications," *IEEE Antennas and Wireless Propagation Letters*, Vol. 15, 1144–1147, 2016.

[45] El Atrash, M., M. A. Abdalla, and H. M. Elhennawy, "A compact highly efficient π-section CRLH antenna loaded with textile AMC for wireless body area network applications," *IEEE Transactions on Antennas and Propagation*, Vol. 69, No. 2, 648–657, Feb. 2021.

[46] Low, J.-H., P.-S. Chee, and E.-H. Lim, "Liquid EBG-backed stretchable slot antenna for human body," *IEEE Transactions on Antennas and Propagation*, Vol. 70, No. 10, 9120–9129, Oct. 2022.

[47] Kamardin, K., M. K. A. Rahim, N. A. Samsuri, M. E. B. Jalil, and I. H. Idris, "Textile artificial magnetic conductor waveguide jacket for on-body transmission enhancement," *Progress In Electromagnetics Research B*, Vol. 54, 45–68, 2013.

[48] Kamardin, K., M. K. A. Rahim, N. A. Samsuri, M. E. Jalil, and M. A. A. Majid, "Textile artificial magnetic conductor waveguide sheet with wire dipoles for body centric communication," *Jurnal Teknologi*, Vol. 64, No. 3, 29–35, 2013.

[49] Kamardin, K., M. K. A. Rahim, N. A. Samsuri, M. E. Jalil, and H. A. Majid, "Transmission enhancement using textile artificial magnetic conductor with coplanar waveguide monopole antenna," *Microwave and Optical Technology Letters*, Vol. 57, No. 1, 197–200, 2015.

[50] Hadarig, R. C., M. E. D. Cos, and F. Las-Heras, "UHF dipole-AMC combination for RFID applications," *IEEE Antennas and Wireless Propagation Letters*, Vol. 12, 1041–1044, 2013.

[51] Pei, R., M. P. Leach, E. G. Lim, Z. Wang, C. Song, J. Wang, W. Zhang, Z. Jiang, and Y. Huang, "Wearable EBG-backed belt antenna for smart on-body applications," *IEEE Transactions on Industrial Informatics*, Vol. 16, No. 11, 7177–7189, 2020.

[52] Agarwal, K., Y.-X. Guo, and B. Salam, "Wearable AMC backed near-endfire antenna for on-body communications on latex substrate," *IEEE Transactions on Components Packaging and Manufacturing Technology*, Vol. 6, No. 3, 346–358, Mar. 2016.

[53] Hong, J. H., C.-W. Chiu, and H.-C. Wang, "Design of circularly polarized tag antenna with artificial magnetic conductor for on-body applications," *Progress In Electromagnetics Research C*, Vol. 81, No. 1, 89–99, 2018.

[54] Chaouche, Y. B., M. Nedil, I. B. Mabrouk, and O. M. Ramahi, "A wearable circularly polarized antenna backed by AMC reflector for WBAN communications," *IEEE Access*, Vol. 10, 12 838–12 852, 2022.

[55] Yang, H., X. Liu, and Y. Fan, "Design of broadband circularly polarized all-textile antenna and its conformal array for wearable devices," *IEEE Transactions on Antennas and Propagation*, Vol. 70, No. 1, 209–220, Jan. 2022.

[56] Yan, S., P. J. Soh, and G. A. E. Vandenbosch, "Low-profile dual-band textile antenna with artificial magnetic conductor plane," *IEEE Transactions on Antennas and Propagation*, Vol. 62, No. 12, 6487–6490, Dec. 2014.

[57] Velan, S., E. F. Sundarsingh, M. Kanagasabai, A. K. Sarma, C. Raviteja, R. Sivasamy, and J. K. Pakkathillam, "Dual-band EBG integrated monopole antenna deploying fractal geometry for wearable applications," *IEEE Antennas and Wireless Propagation Letters*, Vol. 14, 249–252, 2015.

[58] Yan, S., P. J. Soh, and G. A. E. Vandenbosch, "Compact all-textile dual-band antenna loaded with metamaterial-inspired structure," *IEEE Antennas and Wireless Propagation Letters*, Vol. 14, 1486–1489, 2015.

[59] El Atrash, M., M. A. Abdalla, and H. M. Elhennawy, "A wearable dual-band low profile high gain low SAR antenna AMC-backed for WBAN applications," *IEEE Transactions on Antennas and Propagation*, Vol. 67, No. 10, 6378–6388, Oct. 2019.

[60] Gao, G.-P., H.-J. Meng, W.-F. Geng, Z.-H. Dou, B.-K. Zhang, and B. Hu, "A wideband metasurface antenna with dual-band dual-mode for body-centric communications," *IEEE Antennas and Wireless Propagation Letters*, Vol. 21, No. 1, 149–153, Jan. 2022.

[61] Zhang, K., P. J. Soh, and S. Yan, "Design of a compact dual-band textile antenna based on metasurface," *IEEE Transactions on Biomedical Circuits and Systems*, Vol. 16, No. 2, 211–221, Apr. 2022.